

An empirical model for calculation of the collimator contamination dose in therapeutic proton beams

M Vidal^{1,2}, L De Marzi¹, H Szymanowski^{3,4}, L Guinement¹,
C Nauraye¹, E Hierso¹, N Freud^{5,6}, R Ferrand¹, P François¹
and D Sarrut^{5,6}

¹ Institut Curie: Centre de Protonthérapie d'Orsay, 91400 Orsay, France

² Dosisoft, 94230 Cachan, France

³ Deutsches Krebsforschungszentrum (DKFZ), 69121 Heidelberg, Germany

⁴ Physikalisch-Technische Bundesanstalt (PTB), 38116 Braunschweig, Germany

⁵ CREATIS; CNRS UMR5220; Inserm U1044, INSA-Lyon; Université de Lyon, Université Lyon 1, F-69621 Lyon, France

⁶ Léon Bérard Cancer Center, Université de Lyon, F-69373 Lyon, France

E-mail: marie.vidal@nice.unicancer.fr

Received 28 October 2014, revised 30 November 2015

Accepted for publication 1 December 2015

Published 27 January 2016



CrossMark

Abstract

Collimators are used as lateral beam shaping devices in proton therapy with passive scattering beam lines. The dose contamination due to collimator scattering can be as high as 10% of the maximum dose and influences calculation of the output factor or monitor units (MU). To date, commercial treatment planning systems generally use a zero-thickness collimator approximation ignoring edge scattering in the aperture collimator and few analytical models have been proposed to take scattering effects into account, mainly limited to the inner collimator face component. The aim of this study was to characterize and model aperture contamination by means of a fast and accurate analytical model. The entrance face collimator scatter distribution was modeled as a 3D secondary dose source. Predicted dose contaminations were compared to measurements and Monte Carlo simulations. Measurements were performed on two different proton beam lines (a fixed horizontal beam line and a gantry beam line) with divergent apertures and for several field sizes and energies. Discrepancies between analytical algorithm dose prediction and measurements were decreased from 10% to 2% using the proposed model. Gamma-index (2%/1 mm) was respected for more than 90% of pixels. The proposed analytical algorithm increases the accuracy of analytical dose calculations with reasonable computation times.

Keywords: proton therapy, collimator scatter, dose calculation

(Some figures may appear in colour only in the online journal)

1. Introduction

Proton therapy is a state-of-the-art radiotherapy technique allowing high conformity with effective sparing of the surrounding organs at risk. Many proton therapy facilities worldwide currently treat patients with high-energy protons delivered through passive beam lines. With the passive scattering (double scattering (DS)) and uniform scanning (US) techniques, beam shaping is achieved by means of patient-personalized accessories such as collimators and compensators. Collimators are accessories of crucial importance as they are used to tailor the field to the tumor shape in order to spare surrounding critical structures and reduce the dose to healthy tissues, particularly by keeping the width of the lateral penumbra as low as possible. The active beam scanning modality is generally considered to be the best choice to conform the dose to the tumor with little neutron contamination and personalized accessories. However, for ranges greater than 15 cm in water, the lateral penumbra of scanned beams has been shown to be larger than for collimated passive beams (Safai *et al* 2008). Therefore, in addition to the option of optimizing spot size as proposed by Kimstrand *et al* (2008), collimators could be a straightforward and cost-effective solution to also enhance the lateral penumbra for scanned beams.

In order to ideally fulfil their role, collimators should be able to infinitely absorb radiation while presenting no physical thickness. Unfortunately, a non-negligible amount of contamination dose at the vicinity of the field edges is generally observed due to proton penetration and scattering through the collimator material. At the Curie Institute Proton Therapy Center (CIPTC) for instance, slit contamination greater than 10% of the maximum dose was measured in water several centimeters after the exit face of the collimator with spread-out Bragg peaks of clinical energies and patient collimators. In the case of small apertures 20 mm in diameter, some authors have shown, by using Monte Carlo simulations, that this collimator scatter can represent 20% of the total dose immediately behind the aperture. However, this collimator scatter contribution decreases rapidly with depth and almost disappears beyond 15 cm in the patient (van Luijk *et al* 2001). Titt *et al* demonstrated the dosimetric impact of several parameters such as energy, collimator thickness, air-gap, field size and modulation width, which affect the collimator proton scattering distribution (Titt *et al* 2008). This contamination perturbs the dose distribution and consequently the output factors used for the determination of the dose at the calibration point for monitor units (MU) computation (Daartz *et al* 2009, Koch and Newhauser 2010, Zheng *et al* 2011). Collimator contamination should be therefore included in the dose calculation engine of the treatment planning system (TPS), by taking into account the related physical parameters. Moreover, scattered protons lose their energy when they interact with the aperture and low-energy protons are now considered to have a relative biological effectiveness greater than 1.1 (Calugaru *et al* 2011). Consequently the amount of scatter dose and the energy spectrum of the protons emerging from the collimator may need to be evaluated to provide a better understanding of radiobiological issues.

Pencil-beam algorithms are widely and routinely used for dose calculation in TPS (Hong *et al* 1996, Szymanowski *et al* 2001). Recent improvements of pencil-beam algorithms take into account the thickness of the collimator and its influence on penumbra broadening (Slopesma and Kooy 2006, Kanematsu *et al* 2006), but still neglect aperture scattering. Published studies dealing with entrance face collimator contamination have mostly been carried out using

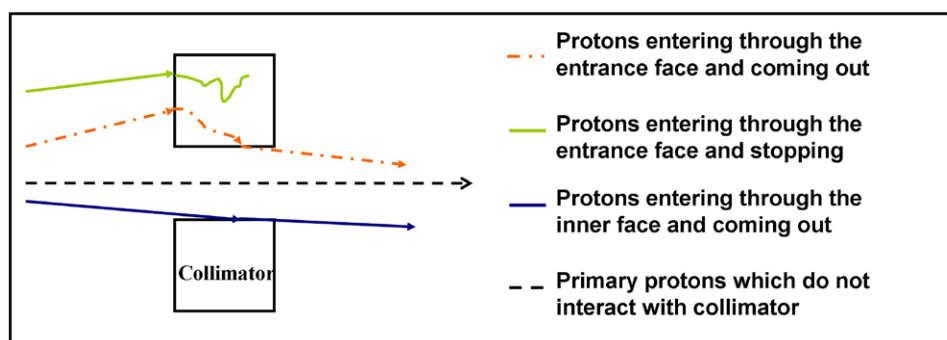


Figure 1. Interaction of protons derived from the inner or entrance face of the collimator.

Monte Carlo simulations, for instance, calculation of scatter kernels to model the proton collimator scatter dose by Kimstrand *et al* (2008). Since Monte Carlo simulations are still very time-consuming, an analytical calculation model of collimator contamination dose is needed, to simply take into account in a simple manner the collimator complex shape and the specific beam line configuration. We have therefore developed an empirical formulation based on a simple mathematical model to calculate dose contamination from collimators of any proton passive beam line. In this paper, we first describe the basic features of the proposed model and the experimental procedure used to derive its beam line specific parameters. The results of parameterization are then presented and discussed for a fixed beam line (FBL) and a gantry beam line (GBL). Finally, the validity of the proposed model is assessed using a second set of simple independent measurements.

2. Material and methods

2.1. Analytical model of the collimator contaminated dose

2.1.1. Basic assumptions of the analytical model. Protons that interact with the collimator can enter the collimator through either the entrance face or the inner face, as depicted in figure 1. Gottschalk and Van Luijk *et al* showed that the protons incident from the entrance face are mostly responsible for perturbation of the on-axis dose, as these protons are back-scattered towards the beam axis into the treatment field (Gottschalk 2004). In contrast, the influence of protons scattered off the inner face is almost negligible (van Luijk *et al* 2001). Van Luijk's conclusions were confirmed by unpublished measurements in water and air on the fixed beam line at CIPTC and led us to focus our study on the entrance face protons.

We assume that the collimator contamination dose can be modeled as an additive scatter contribution within the irradiation field. Equation (1) describes the total dose D^{total} as the sum of D^{prim} , which corresponds to the non-contaminated dose, as calculated by conventional pencil beam algorithms (Szymanowski *et al* 2001), with the scatter collimator contamination (SCC), which is the dose arising from the entrance face collimator scatter contribution.

$$D^{\text{total}} = D^{\text{prim}} + \text{SCC}. \quad (1)$$

2.1.2. Mathematical description of the SCC of a dose distribution. As reported by Titt, the SCC depends on energy, aperture size, air-gap, modulation and collimator thickness (Titt *et al* 2008). In general, the collimator thickness and material are fixed for a given maximal energy beam line configuration. Moreover, for a modulated proton beam, the total dose can be

obtained for any point within the patient as the weighted sum of the dose for pristine Bragg peaks. The proposed analytical model describes the SCC immediately after the collimator, i.e. with a fixed air-gap of 0 cm. Consequently, in a first approximation, we calculated the SCC as a function of energy and aperture size only. Energy was taken into account over the range R of the pristine Bragg peak. Aperture size d was defined as the distance between the calculation point and the collimator edge. We first considered the two-dimensional (2D) configuration (x, z) for the sake of simplicity, and determined the perturbation along the x -axis for an air-collimator semi-infinite interface along the y -axis. We assumed that a field with a complex shape could be decomposed into angular sectors originating from the center of the field, as described by the Clarkson–Cunningham algorithm (Clarkson 1941, Cunningham 1983). The SCC arising from the angular sector i of angle Δ_i can be computed as a dose perturbation of weight $\Delta_i/2\pi$ at distance d_i between the calculation point P and the edge of the angular sector i , as shown in figure 2(a). Each angular sector configuration can be approximated by the half-block collimator depicted on figure 2(b), where parameter d is the distance between the block inner edge and the y -axis represents the distance between the collimator segment considered and the beam axis.

Qualitatively, collimator scattering is closely related to dose perturbation by a thick inhomogeneity. We empirically modeled collimator scatter contamination by defining a secondary effective source modeling the protons that are scattered from the collimator entrance (red dashed line in figure 1). Because of the multiple Coulomb scattering processes within the collimator and based on an experimental set of measurements, we assume that the fluence of the narrow contamination beam at the exit of the collimator mainly exhibits a Gaussian shape.

Based on the aforementioned assumptions, we therefore chose to approximate the entrance face collimator scatter contribution of one angular sector of aperture size for a pristine Bragg peak proton beam, for the 1D configuration, by a single 1D Gaussian function. Equation (2) describes the collimator contamination $\text{SCC}_{R,d}$ as a Gaussian function of the transverse dimension x and the depth z in the target, as only one transverse dimension x is considered here

$$\text{SCC}_{R,d}(x, z) = A_{R,d}(z) \times \exp\left(-\left[\frac{x - \lambda_{R,d}(z)}{\sqrt{2}\sigma_{R,d}(z)}\right]^2\right). \quad (2)$$

R corresponds to the initial range of the proton beam. d is the distance of the calculation point P of coordinates (x, z) to the collimator segment. $A_{R,d}$ represents the amplitude of the scatter dose distribution function. $\lambda_{R,d}$ is the center of the distribution and $\sigma_{R,d}$ its width.

2.1.3. Parameterization of the analytical model based on experimental data. Based on the assumption that the total contaminated dose can be approximated as the sum of the non-contaminated dose and the collimator scatter dose, the scatter contribution can be extracted from lateral dose measurements in the presence of a collimator as follows:

$$\text{SCC}_{R,d}^{\text{exp}}(x, z) = D_{R,d}^{\text{mes}}(x, z) - D_{R,d}^{\text{prim}}(x, z). \quad (3)$$

$D_{R,d}^{\text{mes}}(x, z)$ can be obtained from measurements of the lateral dose distribution in water in the presence of the collimator. $D_{R,d}^{\text{prim}}(x, z)$ is the primary dose, the ideal non-contaminated lateral dose profile. It can be calculated with conventional pencil beam algorithms, in our case the algorithm described by Szymanowski *et al* (2001).

Parameters $A_{R,d}$, $\lambda_{R,d}$ and $\sigma_{R,d}$ of equation (2) theoretically depend on the initial energy (represented by the range R) and the aperture size d . The values of these parameters can be extracted from the 2D measurements. At each depth z , the experimental data $\text{SCC}_{R,d}^{\text{exp}}$ was

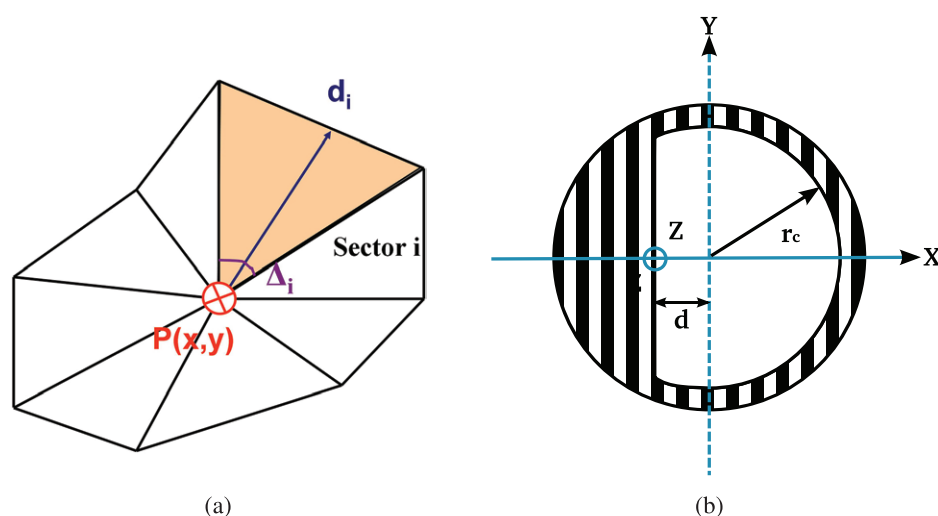


Figure 2. (a) Dose computation in P for a complex field shape by decomposing the field into angular sectors derived from the dose calculation point P at a distance d_i from the edge of the angular sector i . (b) Schematic beam's eye view of the designed divergent 'half-block' collimator. d is the distance between the central beam axis and the straight inner edge of the half-block collimator, while r_c is the maximum radius of the half-block collimator outer edge.

fitted to a Gaussian distribution using optimization procedures based on the Levenberg–Marquardt algorithm (Marquardt 1963), and for all (R, d) configurations we got the values of the three parameters. Their variation laws in function of depth can be then extrapolated for any beam set-up.

2.2. Experimental set-up and Monte Carlo simulations

2.2.1. Measurements.

Measurements were performed at CIPTC with an FBL and a GBL. The FBL is a horizontal passive beam line with a fixed initial energy beam of 201 MeV delivered by a synchrocyclotron, while the GBL is equipped with a universal nozzle in a gantry room, connected to a cyclotron delivering a 230 MeV proton beam (IBA, Belgium). Both beam lines were set to DS mode, meaning that the range of the different Bragg Peaks was adjusted with the range binary filter, while the second scatterer enlarged the beam size laterally and the beam was depth-modulated by means of dynamic wheels. Set-ups of the two lines were similar; however, different second scatterers have been designed to be used with the maximum required field size, which depends on the treatment location. For example, FBL is dedicated to head or skull base tumours, and is equipped with a smaller second scatterer leading to smaller maximum ranges, field sizes and lateral penumbra than GBL. At the end of both beam lines, divergent brass collimators, personalized to each patient, are used to obtain a smaller lateral penumbra in the patient (Oozeer *et al* 1997). Divergent collimators are designed as a function of the distance between the collimator edge and the patient isocenter, the virtual source axis distance and the collimator thickness in order to more accurately fit beam divergence.

For the determination of the scatter contamination function, special divergent collimators were designed to reproduce the semi-infinite interface conditions described in the previous section. Wide brass circular collimators, 5 cm and 6 cm thick, for FBL and GBL, respectively,

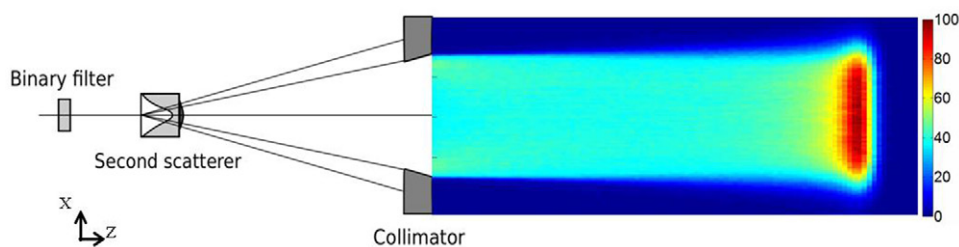


Figure 3. Experimental set up for 2D dose maps measurements with the fixed beam line, including a binary filter, a second scatterer, and finally a collimator (half-blocked or circular).

featuring a block partially hiding the irradiation field were manufactured as shown in figure 2(b). Their radius r_c was defined such that the contribution from the circular collimator was negligible. The block was parallel to the y -axis and we measured the contamination generated at the inner edge of the half-block collimator situated at the distance d of the point of interest.

On the FBL, measurements of the lateral dose profiles were performed in a water tank positioned immediately after the collimator. On the GBL, the gantry angle was set to 0° and the water tank was positioned below the nozzle, without an air-gap between the collimator and the water surface. The water level was also checked regularly during the experimental sessions.

In order to extract the parameters of the scatter contamination function, and to take into account the beam specificities between the rooms (different maximum and mean clinically relevant field sizes and ranges obtained by different second scatterer dimensions), the aperture size d was varied with values [5, 10, 15, 20, 30] mm and [10, 20, 30, 40] mm for FBL and GBL, respectively. The beam ranges investigated ranged from 122 mm to 207 mm and from 155 mm to 219 mm water equivalent for pristine Bragg peaks for FBL and GBL, respectively. Lateral dose distributions along the x -axis were measured at 5 mm increments with a pin-point CC01 ionization chamber (*IBA dosimetry*) to improve the signal-to-noise ratio while maintaining good precision. In order to build a 2D dose distribution as depicted in figure 3, profiles were acquired at 3 mm depth intervals.

Additional measurements were performed in order to evaluate the proposed contamination model for simple radial geometries. Validation was carried out for conventional circular collimators with aperture diameters equal to 30 and 40 mm for a range of 169 mm on the FBL, and aperture diameters of 40 and 80 mm for ranges of 198 mm and 219 mm on the GBL. We compared these measurements with the dose calculation for full circular collimators using the complex field approach depicted in figure 2(a).

The calculated and measured 2D dose distributions were normalized at the Bragg peak maximum. The difference between the calculated dose profile D_{calc} and the measured dose profile D_{mes} was expressed as a percentage and computed as follows: $\text{Diff} = (D_{\text{calc}} - D_{\text{mes}})/D_{\text{mes}} \times 100$.

A comparison based on gamma index computation (Low *et al* 1998) was performed for 2D dose distributions. The computation of the gamma index was restricted to an area of interest which includes all depth range (up to 10 cm in depth), and which is 2 cm wide starting from the inner edge of the half-block collimator, in order to compare the analytical model computation and measurement of the entrance face contamination only. The gamma index ($\Delta d_{\text{max}} = 1$ mm, $\Delta D_{\text{max}} = 2\%$) map was calculated using the local method in the area of interest described above for half-block collimators, and in the whole field for circular collimators.

2.2.2. Monte Carlo simulations. Monte Carlo simulations were performed in order to evaluate the variation of the SCC function parameters A , λ and σ as a function of various parameters that cannot be easily measured, and to obtain information for the design of experimental half-block collimators. Because of the beam lines similarity, we assumed that the model of SCC is the same, with different values of the SCC function parameters. Consequently, only the FBL was simulated with the GEANT4-based platform GATE 6.1 (Jan *et al* 2011, Sarrut *et al* 2014). All beam elements, except the monitor chambers, were defined. The beam source was described as proposed by Grevillot *et al* (2011) for scanned proton beams and was adjusted for DS. The nominal beam energy was set at 201 MeV with an energy straggling of 0.95 MeV (energy spectrum defined as a Gaussian distribution) and the lateral dispersion was set at 4 mm while the angular distribution was equal to 5 mrad. This set-up reproduced, with an uncertainty of less than 1%, the lateral field size and the proton range of FBL complete dose distributions.

Monte Carlo simulations showed that the distance r_c , between the outer collimator edge and the central beam axis, should not be less than 3 cm to ensure that no contamination contribution derived from that edge of the circular collimator perturbs the acquisition on the measurement point. For fully circular apertures with a radius r_c less than 3 cm, the observed contamination is sometimes not visible because of the overlap of the whole cylindrical aperture contamination contributions, which give a uniform distribution but with an offset caused by the scattering contamination. r_c was therefore set at 6 cm for the manufactured half-block collimators used for experimental measurements.

Additional Monte Carlo simulations of the FBL were also used to evaluate the variation of SCC parameters A , λ and σ in the function of nominal energy (170–210 MeV), Gaussian energy spectrum width (0.2–3 MeV) and beam divergence (0–5 mrad), in order to validate our analytical model.

3. Results

3.1. Validation of model parameterization

Figure 4 illustrates the optimization procedure for one range and aperture size configuration ($R = 20.7$ cm, $d = 15$ mm): the points show the value of the three parameters $\sqrt{(K/A_{R,d})}$, $\lambda_{R,d}$ and $\sigma_{R,d}$ for each depth z , where K is a dose fluence coefficient in [$\text{Gy}\cdot\text{cm}^2$] to express SCC in [Gy]. The functions $A_{R,d}(z)$, $\lambda_{R,d}(z)$ and $\sigma_{R,d}(z)$ were then linearly fitted in function of depth with the least-squares method with a correlation coefficient higher than 95%, 80% and 70%, respectively, for all configurations (R, d).

We found that, for various values of beam range and aperture size, the amplitude $A_{R,d}$ of the Gaussian distribution function depended on depth z as a linear function of $1/z^2$. This means that contamination may be considered to be an extended source located in the collimator. We defined the slope and y-intercept as functions of range and aperture size, respectively: $m(R, d)$ and $n(R, d)$ as shown in equation (4), and the dose fluence coefficient K in [$\text{Gy}\cdot\text{cm}^2$]

$$A_{R,d}(z) = K \times \frac{1}{(m(R, d) \times z + n(R, d))^2}. \quad (4)$$

Similarly, we found that the position $\lambda_{R,d}$ of the center of the Gaussian distribution also depended linearly on depth. $\lambda_{R,d}$ is purely a geometrical factor and depends on aperture size but not on beam energy, as confirmed by Monte Carlo simulations performed in this work.

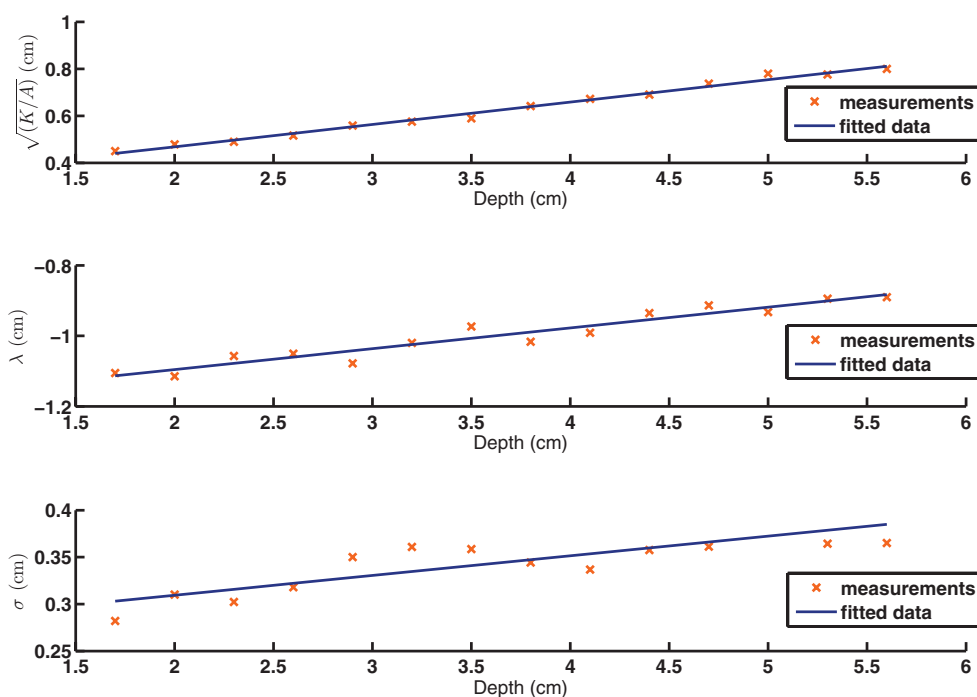


Figure 4. Parameter fitting: $\sqrt{K/A_{R,d}}$, $\lambda_{R,d}$ and $\sigma_{R,d}$ of the Gaussian SCC, function of depth z for range $R = 20.7$ cm and distance $d = 15$ mm.

Therefore position $\lambda_{R,d}$ of the center of the contamination distribution can be expressed as described in equation (5).

$$\lambda_{R,d}(z) = \lambda_d(z) = k(d) \times z + l(d) \tag{5}$$

where $k(d)$ and $l(d)$ are linear functions of aperture size d .

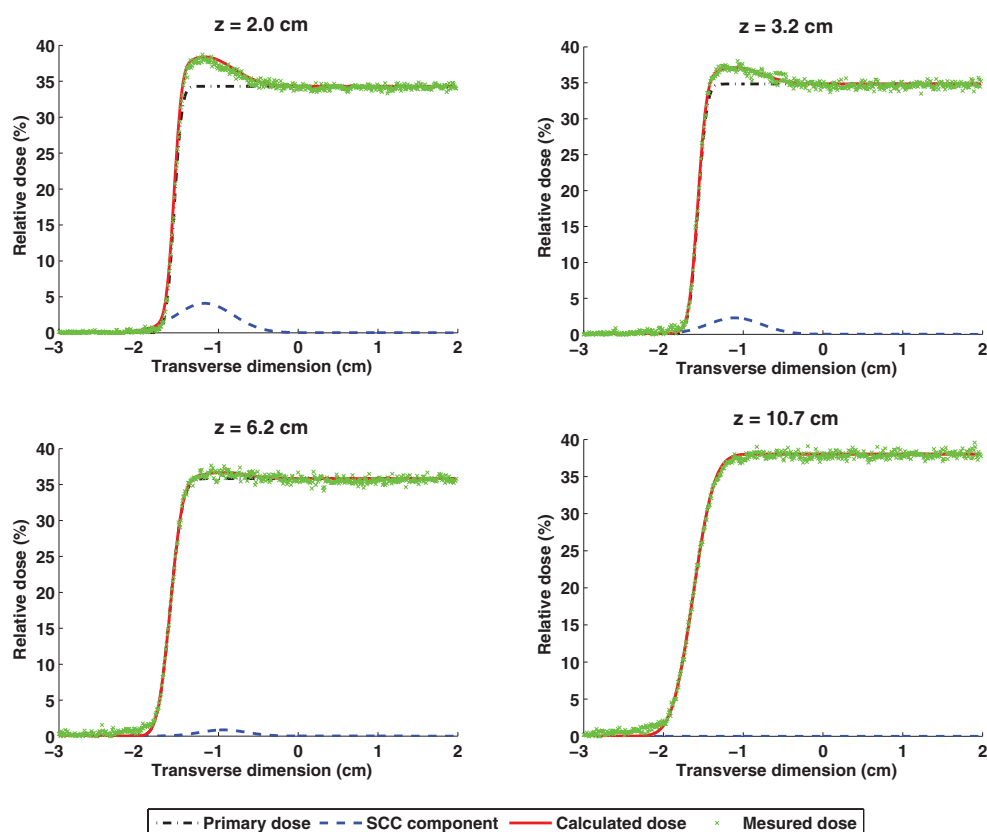
The values experimentally extracted for $\sigma_{R,d}$ showed that $\sigma_{R,d}$ can be considered to be constant in a first approximation. It was set to 0.31 cm and 0.36 cm for the energy ranges considered of FBL and GBL respectively.

The dependence of parameters A , λ and σ on energy and aperture was also assessed by Monte Carlo simulations of the FBL. In particular, simulation of the variation of A , λ and σ as a function of nominal energy (170–210 MeV), Gaussian energy spectrum width (0.2–3 MeV) and beam divergence (0–5 mrad) was independently evaluated and was found to be in agreement with the experimental results. This study shows that parameter A varies by less than 2% with beam divergence and the width of the energy spectrum. Moreover, beam energy affects the values of parameters λ and σ by less than 3%. Nevertheless, λ varies with the beam divergence angle which is only to be expected, as it is a geometric parameter, but the variation does not exceed 10% of the value of λ . Finally, the value of σ should be influenced by both the width of the energy spectrum and the beam divergence angle, but these two effects appear to compete with each other and stabilize the σ value as a constant.

The parameterizations described in equations (4) and (5) were implemented in the proposed model. The functions $m(R, d)$, $n(R, d)$, $k(d)$ and $l(d)$ are given in table 1 for FBL and GBL. $n(R, d)$ and $l(d)$ are expressed in cm, and $m(R, d)$ and $k(d)$ numerical values are given for z expressed in cm.

Table 1. Functions $m(R, d)$, $n(R, d)$, $l(d)$ and $k(d)$ which describe the parameterization of the SCC model for FBL and GBL.

FBL	GBL
$m(R, d) = 0.3265$	$m(R, d) = 0.0033$
$n(R, d) = -0.0129 \times (R + d) + 0.3265$	$n(R, d) = -0.0030 \times (R + d) + 0.9553$
$k(d) = 0.0593$	$k(d) = 0.0540$
$l(d) = -0.9924 \times d + 0.3562$	$l(d) = -0.0253 \times d + 7.3580$

**Figure 5.** Comparison of 1D profiles of the measured and analytically computed dose profiles for the configuration ($d = 20$ mm, $R = 16.9$ cm) of the FBL at several depths. The SCC function and the primary dose are also represented for each depth. The dose is normalized at the maximum of the Bragg peak.

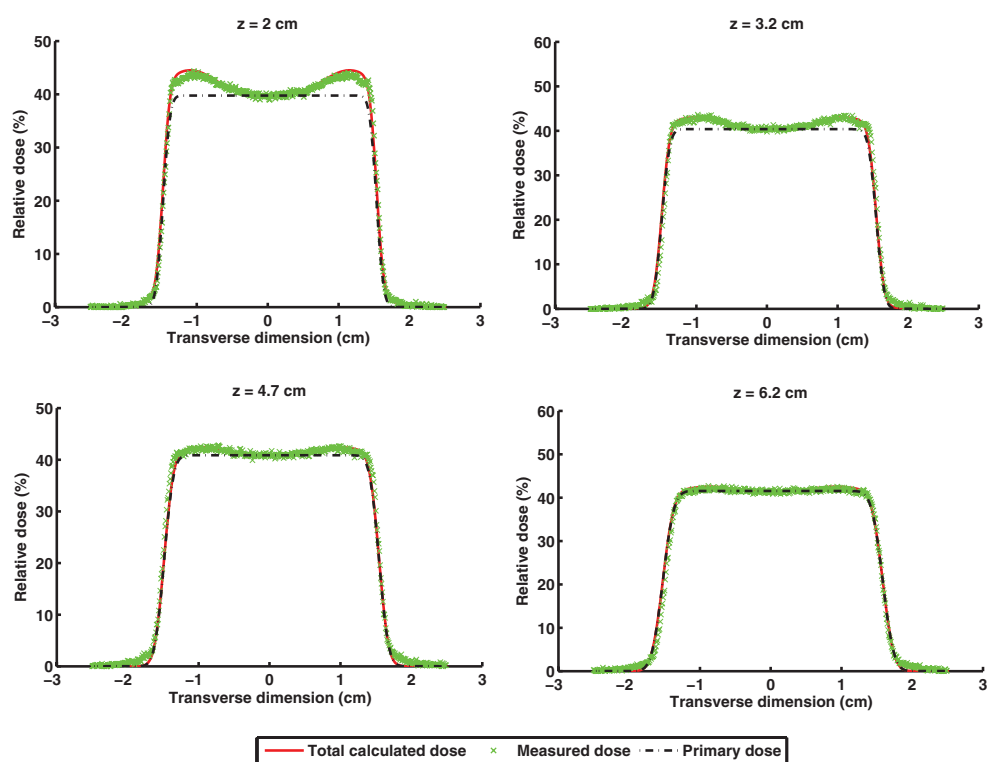
We first verified the ability of the model at reproducing the experimental data the parameterizations were based upon. The scatter contamination function was evaluated for all measurement configurations with partially blocked collimators. The computed and measured 2D total dose distributions were then compared. For all configurations, the difference between both dose distributions ranks from 1% to 4% of the measured dose for both beam lines. As an example, figure 5 shows lateral dose profiles for an aperture size of $d = 20$ mm and a beam range $R = 169$ mm in water for FBL. From the edge of the collimator, from $x = -20$ mm

Table 2. Percentage of pixels with gamma index (2%/1 mm) less than 1.0 by comparing computed to measured dose distributions for all measured (R , d) configurations of the FBL.

d (cm) / R (cm)	12.2 cm	13.4 cm	15.6 cm	16.9 cm	18.2 cm	20.7 cm
0.5 cm	—	99.6%	—	100%	—	99.7%
1.0 cm	99.8%	99.2%	—	99.4%	—	99.3%
1.5 cm	100%	100%	100%	99.2%	99.8%	99.7%
2.0 cm	99.6%	99.6%	—	99.7%	—	99.3%
3.0 cm	—	99.1%	—	—	—	98.4%

Table 3. Percentage of pixels with gamma index (2%/1 mm) less than 1.0 by comparing computed to measured dose distributions for all measured (R , d) configurations of the GBL.

d (cm) / R (cm)	15.5 cm	19.8 cm	21.9 cm
1.0 cm	88.3%	—	93.4%
2.0 cm	93.0%	92.1%	93.6%
3.0 cm	90.5%	95.3%	94.5%
4.0 cm	96.4%	96.9%	95.4%

**Figure 6.** Comparison of the measured and analytically computed dose profiles for the configuration 30 mm diameter circular collimator at a proton beam range $R = 169$ mm. The primary dose, which is the actual TPS dose calculation without contamination computation, is also represented. The dose distributions are normalized to the maximum of the Bragg peak.

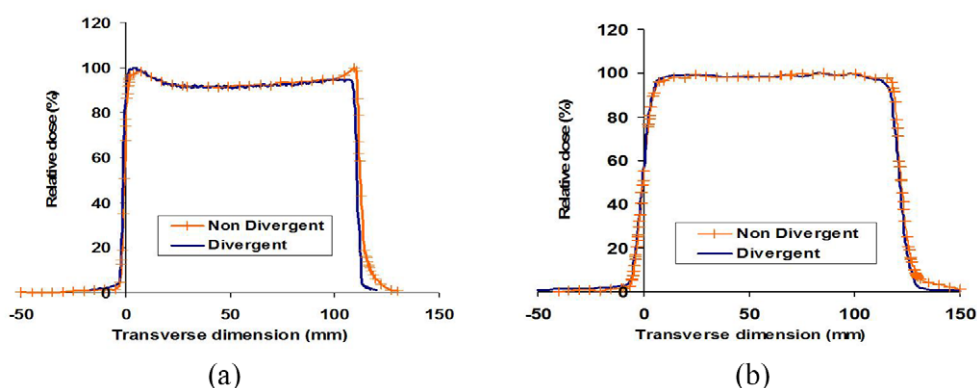


Figure 7. Comparison of dose lateral profiles obtained with a divergent and a non-divergent collimator for a range of 21.7 cm and a radius of 110 mm at two different depths: $z = 0$ cm (a) and $z = 20$ cm (b).

(equivalent to $d = 20$ mm) to $x = 15$ mm, the mean difference is nearly below 2% of the measured dose, while it is above 10% with conventional pencil beam algorithms.

The gamma index calculation in the half-blocks contamination area of interest revealed a high level of agreement between the computed and measured 2D total dose distributions for all conditions of range R and distance d . Concerning the FBL, the 1.5 cm half-block collimator was studied for all measured ranges, while only the 13.4, 15.6 and 20.7 cm range measurements were analyzed for all half-block aperture sizes. With the partially blocked field configuration, i.e. mimicking slab geometry conditions, the chosen parameterization yielded satisfactory results. The percentage of pixels with a 2%/1 mm gamma index less than 1.0 ranged from 98.4% to 100% for the FBL, as shown in table 2, and from 88.3% to 96.9% for the GBL as shown in table 3.

3.2. Validation of the model

We compared, computed and measured 2D dose distribution with circular collimators for both beam lines. Figure 6 presents an example of the comparison between the measured and computed dose distribution obtained on the FBL with a 30 mm diameter circular collimator with a range of 169 mm, for different depths z . The new collimator contamination model significantly reduces the discrepancies between the dose calculation model and measurements from 10% to 1%. The 2%/1 mm gamma index calculation over the whole field shows that almost 94% and 93% of the pixels respect the criteria for the 30 mm and 40 mm radius circular collimators respectively on the FBL for range equal to 169 mm.

Concerning the GBL, 2%/1 mm gamma index values range between 88.6% and 90.5% for dose distributions in the presence of circular collimators 40 mm and 80 mm in diameter for pristine Bragg peaks of ranges equal to 19.8 cm and 21.9 cm.

For both beam lines, collimator contamination was relevant for depths less than 6 cm, 8 cm and 10 cm for pristine Bragg peaks with ranges of 169 mm, 198 mm and 219 mm, respectively. Moreover, collimator scattering contamination is observable for ranges greater than 122 mm and 155 mm for FBL and GBL respectively because of the use of divergent collimators. Indeed the use of divergent collimators considerably reduces collimator contamination, from both inner and entrance faces of the collimator, compared to usual non-divergent collimators.

In particular, figure 7 compares lateral profiles on the GBL for a beam range of 211 mm and a half-blocked collimator with a radius of 110 mm. A difference of 9% of the maximum dose on the exterior side is observed depending on whether the collimator is divergent or not. Measurements on both beam lines showed that for ranges less than 150 mm and 120 mm in water equivalent for pristine Bragg peaks of GBL and FBL respectively, the remaining entrance face contamination is considerably decreased (less than 2% of the maximum dose) when using divergent collimators.

For circular collimators, the largest discrepancies between measurements and the analytical model were observed at the collimator edge of the lateral distributions with increasing depth. The observed difference, that represents up to 5% of the measured dose, does not impact the 80%–20% penumbra. Monte Carlo simulations suggested that it could be due to the inner face proton contamination, and this contamination is not taken into account by the SCC function. Moreover, a discordance of up to 2% was also observed for entrance face contamination, particularly for the smallest depths. This is due to day-to-day fluctuations of beam tuning, affecting beam uniformity. These fluctuations depend on factors such as beam transport regulation and ion source current.

4. Discussion

The proposed model was evaluated for two different beam lines (FBL and GBL). In order to achieve beam lateral uniformity conditions for all values of the range, different second scatterer dimensions were used for the FBL and the GBL, which induced slight variations of the energy spectrum and discrepancies between the virtual SAD of about 5.4 m and 2.3 m for FBL and GBL, respectively. SCC is indeed influenced by these variations. However, the proposed analytical model is able to take these variations into account by the optimization of SCC function parameters and the general form of the SCC function as a 2D Gaussian is valid for both beam lines.

Since the virtual SAD for the FBL is very large, the beam is almost parallel to the beam axis and has a slight divergence, unlike the GBL beam which shows a larger divergence since its SAD is approximately one half of the FBL SAD's. Measurements therefore generally showed that the collimator contamination value was smaller for the GBL than for FBL, because more protons interact and scatter at the collimator edge for a parallel beam than for a divergent beam, although the collimator is divergent and conforms the beam divergence. Moreover, GBL collimators are thicker than FBL collimators (6 cm versus 5 cm for FBL) and more protons are absorbed by brass, which may explain the lower contamination for the GBL.

We also showed that the use of divergent collimators can help to reduce contamination values for modalities using collimators, particularly DS and US. Contamination of the GBL can be reduced by about 9%, resulting in very low contamination for low ranges. SCC reaches only a few percent (3%) of the maximum dose for a beam range of 155 mm and an aperture of 10 mm. Consequently the number of pixel percentages below the 2%/1 mm gamma index is less than 90%, and better results were observed for the highest range of 219 mm. The best results were obtained for the largest ranges, because under these conditions, the SCC is relatively higher and more easily measured. Moreover, since the SCC is higher for the FBL than for the GBL, a larger number of pixels below the 2%/1 mm gamma index were obtained for the FBL.

Moreover, the SCC influences the whole dose distribution as far as the Bragg peak depth (van Luijk *et al* 2001), but contamination is significant (above 1% of the maximum dose) only

in the first few centimeters: on the FBL, contamination was relevant for the first 6 cm for a pristine Bragg peak of 16.9 cm range, while on the GBL, it was relevant for the first 8 cm and 10 cm for pristine Bragg peaks of 19.8 cm and 21.9 cm range, respectively.

This study was devoted to the prediction of the macroscopic effect of collimator contamination on dose distribution. Our experiments led us to perform simple parameterization of the results, which provided efficient modeling of contamination. Nevertheless collimator contamination is a complex issue, as penetration of protons through the collimator gives rise to a wide spectrum of energies and angular dispersions. Monte Carlo simulations such as those performed by van Luijk *et al* (2001), Titt *et al* (2008) and Gottschalk (2004) are therefore still necessary to provide a better understanding of the processes occurring at a microscopic level. Monte Carlo simulations may be used, for example, to investigate the behavior of the SCC function in the presence of materials other than water, such as air, to model the air-gap between the collimator and the patient, a compensator and patient heterogeneities, which were not considered in the present work. Matsinos, for example, proposed a model which takes into account the second scatterer and the nozzle equivalent thickness changes in beam lines similar to the GBL (Matsinos 2008). More generally, we are planning further studies more closely resembling actual patient treatment configuration, e.g. involving spread out Bragg peaks, divergent and non divergent complex collimators, before applying the model in routine clinical practice.

Our measurements were performed for DS beam lines, but collimators are also used in US, and are already used for pencil beam scanning to improve lateral penumbra (Safai *et al* 2008, Hyer *et al* 2014). When using these beam modalities, the collimator also perturbs the dose distribution. A similar method could therefore be adapted to take the collimator contamination into account. The results presented here are sufficiently satisfactory to combine analytical description of the SCC function with the calculation of MU in a next step. The output factors will then take into account the effect of collimator contamination for each treatment field and the MU computation will be improved.

5. Conclusion

In this study, an empirical model to describe collimator dose contamination of two different therapeutic proton passive beam lines was proposed. Including the SCC model in analytical dose calculation allows computation of dose distributions with an error of less than 2% of the relative dose (normalized to the Bragg peak maximum) at shallow depths, against 10% without the SCC model, for both horizontal and gantry beam lines. Further studies are needed to allow application of the new model to complex geometrical patient configurations. It is based on an important bench of experimental data for various energies and aperture sizes for two different proton beam lines, and on Monte Carlo simulation results but it does not rely on theoretical assessments. However, we believe that the experimental method developed in this paper to model collimator contamination can be applied to several types of passive beam line, without time-consuming Monte Carlo simulation of the detailed beam line and could be extended to other treatment modalities, such as US or pencil beam scanning.

Acknowledgments

This work was performed in part within the framework of the LABEX PRIMES (ANR-11-LABX-0063) of Université de Lyon, within the 'Investissements d'Avenir' (ANR-11-IDEX-0007) program operated by the French National Research Agency (ANR), and was

supported in part by the Lyric grant INCa-DGOS-4664. This work was also supported by the French project ‘Cancéropôle Ile de France’ entitled ‘Towards dynamic protontherapy’ and by the French company Dosisoft. The authors do not have any conflict of interest.

References

- Calugaru V, Nauraye C, Noël G, Giocanti N, Favaudon V and Méglin-Chanet F 2011 Radiobiological characterization of two therapeutic proton beams with different initial energy spectra used at the institut curie proton therapy center in orsay *Int. J. Radiat. Oncol. Biol. Phys.* **81** 1136–43
- Clarkson J R 1941 A note on depth doses in fields of irregular shape *Br. J. Radiol.* **14** 265–8
- Cunningham J 1983 *The Physics of Radiology* 4th edn (Springfield, IL: Charles C Thomas)
- Daartz J, Engelsman M, Paganetti H and Bussiere M R 2009 Field size dependence of the output factor in passively scattered proton therapy: influence of range, modulation, air gap, and machine settings *Med. Phys.* **36** 3205–10
- Gottschalk B 2004 *Passive Beam Spreading in Proton Radiation Therapy (Draft Oct 2004)* Available at <http://gray.mgh.harvard.edu/attachments/article/212/pbs.pdf>
- Grevillot L, Bertrand D, Dessy F, Freud N and Sarrut D 2011 A Monte Carlo pencil beam scanning model for proton treatment plan simulation using GATE/GEANT4 *Phys. Med. Biol.* **56** 5203–19
- Hong L, Goitein M, Bucciolini M, Comiskey R, Gottschalk B, Rosenthal S, Serago C and Urie M 1996 A pencil beam algorithm for proton dose calculations *Phys. Med. Biol.* **41** 1305–30
- Hyer D E, Hill P M, Wang D, Smith B R and Flynn R T 2014 A dynamic collimation system for penumbra reduction in spot-scanning proton therapy: proof of concept *Med. Phys.* **41** 091701
- Jan S et al 2011 GATE V6: a major enhancement of the gate simulation platform enabling modelling of ct and radiotherapy *Phys. Med. Biol.* **56** 881–901
- Kanematsu N, Akagi T, Takatani Y, Yonai S, Sakamoto H and Yamashita H 2006 Extended collimator model for pencil-beam dose calculation in proton radiotherapy *Phys. Med. Biol.* **51** 4807–17
- Kimstrand P, Traneus E, Ahnesjö A and Tilly N 2008 Parametrization and application of scatter kernels for modelling scanned proton beam collimator scatter dose *Phys. Med. Biol.* **53** 3405–29
- Koch N C and Newhauser W D 2010 Development and verification of an analytical algorithm to predict absorbed dose distributions in ocular proton therapy using Monte Carlo simulations *Phys. Med. Biol.* **55** 833–53
- Low D A, Harms W B, Mutic S and Purdy J A 1998 A technique for the quantitative evaluation of dose distributions *Med. Phys.* **25** 656–61
- Marquardt D W 1963 An algorithm for least-squares estimation of nonlinear parameters *J. Soc. Ind. Appl. Math.* **11** 431–41
- Matsinos E 2008 Collimator effects in proton planning arXiv: 0811.1076
- Oozeer R, Mazal A, Rosenwald J C, Belshi R, Nauraye C, Ferrand R and Biensan S 1997 A model for the lateral penumbra in water of a 200 MeV proton beam devoted to clinical applications *Med. Phys.* **24** 1599–604
- Safai S, Bortfeld T and Engelsman M 2008 Comparison between the lateral penumbra of a collimated double-scattered beam and uncollimated scanning beam in proton radiotherapy *Phys. Med. Biol.* **53** 1729–50
- Sarrut D et al 2014 A review of the use and potential of the GATE Monte Carlo simulation code for radiation therapy and dosimetry applications *Med. Phys.* **41** 064301
- Slopsema R L and Kooy H M 2006 Incorporation of the aperture thickness in proton pencil-beam dose calculations *Phys. Med. Biol.* **51** 5441–53
- Szymanowski H, Mazal A, Nauraye C, Biensan S, Ferrand R, Murillo M C, Caneva S, Gaboriaud G and Rosenwald J C 2001 Experimental determination and verification of the parameters used in a proton pencil beam algorithm *Med. Phys.* **28** 975–87
- Titt U, Zheng Y S, Vassiliev O N and Newhauser W D 2008 Monte Carlo investigation of collimator scatter of proton-therapy beams produced using the passive scattering method *Phys. Med. Biol.* **53** 487–504
- van Luijk P, van't Veld A A, Zelle H D and Schippers J M 2001 Collimator scatter and 2D dosimetry in small proton beams *Phys. Med. Biol.* **46** 653–70
- Zheng Y, Ramirez E, Mascia A, Ding X, Okoth B, Zeidan O, Hsi W, Harris B, Schreuder A N and Keole S 2011 Commissioning of output factors for uniform scanning proton beams *Med. Phys.* **38** 2299–306